Light Metal Propellant Hall Thrusters

IEPC-2009-138

Presented at the 31st International Electric Propulsion Conference,
University of Michigan • Ann Arbor, Michigan • USA
September 20 – 24, 2009

James Szabo,[1] Mike Robin,[2] John Duggan, [3]
Busek Co. Inc, Natick, MA, 01760, USA

Richard R. Hofer[4]
Jet Propulsion Laboratory, California Institute of Technology, Pasadena, CA, 91109, USA

Abstract: The feasibility of using magnesium (Mg) and zinc (Zn) vapor as Hall Effect Thruster propellant was proven. Mg and Zn are plentiful, non-toxic, low cost alternatives to xenon and krypton. Because Zn and Mg are lightweight, specific impulse of 2500-4200 s is possible at discharge voltages of 300 V, enabling the use of existing power processors for a high specific impulse system. In the program that is described, Busek demonstrated both Zn and Mg Hall thruster systems. The Zn configuration was very stable, enabling measurements of thrust, discharge oscillations, and the variation of current with magnetic field strength. The measured thrust to power with a discharge potential of 250 V was as high as 49 mN/kW. The specific impulse at 250 V, 1-kW peaked at >2100 s, +/- 16%. The breathing mode oscillation was 21-23 kHz. The Mg configuration was less fully characterized. Busek also developed and characterized under vacuum a novel wire-based feed system that can provide precise control of Zn and Mg feed rates in future thruster systems. This system also enables long term, low pressure, ambient temperature propellant storage. Zn vaporization rates up to 3 mg/s were demonstrated. Mg sublimation rates up to 0.84 mg/s were also demonstrated.

Nomenclature

e	=	charge of an electron, 1.6×10^{-19} C
g_0	=	gravitational constant at Earth's surface, 9.81 m/s^2
I_d	=	discharge current
I_m	=	magnet current
I_{sp}	=	specific impulse (effective exhaust velocity divided by g)
$\dot{m}$	=	anode mass flow rate/metal vapor production rate
M	=	mass of an ion
M_r	=	residual mass
P_d	=	discharge power
t	=	time
T	=	thrust; temperature
V_{sc}	=	velocity of a spacecraft
V_d	=	potential difference applied by the discharge power supply
Z	=	mean ion charge

[1] Chief Scientist for Hall Thrusters, jszabo@busek.com
[2] Research Engineer, mike@busek.com
[3] Technician
[4] Senior Engineer, Electric Propulsion Group, richard.r.hofer@jpl.nasa.gov

η_e = electrical efficiency

η_t = thrust (anode) efficiency

η_u = gas utilization efficiency

I. Introduction

THIS paper describes the results of a Phase I Small Business Innovative Research (SBIR) program sponsored by NASA in which Busek Co. Inc. proved the feasibility of using magnesium (Mg) and zinc (Zn) vapor as Hall Effect Thruster (HET) propellant.

A. Motivation

For over four decades, the noble gas xenon has been the propellant of choice for HETs and their cousins, ion engines. Its advantages are that it is inert, storable, relatively heavy, and easy to ionize. However, xenon is scarce and, hence, extraordinarily expensive to procure. Furthermore, because Xe condenses only at very low temperatures, test facilities are expensive to operate. Lifetime testing can cost millions of dollars. On orbit, xenon must be stored at high pressure in expensive, temperature controlled propellant tanks.

There are also performance related problems with xenon. To reach I_{sp} > 3000 with a xenon Hall thruster, discharge potentials greater than V_d=700 V are required. This introduces several additional demerits. First, the high voltages required by Xe to reach I_{sp} > 3000 are not supported by any off-the-shelf (flight qualified) Hall thruster power processors. Second, channel erosion rates increase significantly when the ions are heavier and more energetic, decreasing the lifetime of the thruster. Third, since running at high voltage generally entails running at lower gas densities, the propellant utilization efficiency is not as high as it could be.

Krypton is a viable, lighter weight, noble gas alternative, but testing at NASA,[1] as well as at Busek shows peak efficiencies that are 0-10% lower in absolute terms than possible with xenon. This is certainly related to krypton's electron impact ionization cross section, which is smaller than that of xenon, as well as its first ionization energy, which is higher than that of xenon. Furthermore, krypton is also relatively scarce and expensive to procure, and like xenon it requires expensive, cryogenically pumped test facilities. Finally, Kr stores at lower density than xenon. Busek is actively searching for better alternatives.

B. Propellant Options

The literature identifies many propellant options.[2, 3, 4] Table 1 lists key properties of some that are most attractive. This table includes Mg, Zn, Kr, I, Xe, Cs, and Bi. The five additional propellants introduced by Table 1 are all considered to be condensable. We first consider the three propellants that are not the subject of this paper. These are iodine, cesium, and bismuth.

Table 1. Properties of various potential Hall thruster propellants.

Element	Mg	Zn	Kr	I	Xe	Cs	Bi
Atomic Mass	24.3	65.4	83.8	126.9	131.3	132.9	209.0
Ionization Properties							
First Ionization Potential (eV)	7.64	9.4	14	10.4	12.1	3.9	7.3
Peak X-section (10^-16 cm^2)	8.0	5.0	3.7	6.0	5.0	12.0	8.0
Thermophsical Properties							
Storage density (gm/cm^3)	1.7	7.1		4.9	1.6	1.9	9.8
Freezing Point (C)	650	420		113.7		39	271
Boiling Point @ 0.1 torr, C	509	408		12		200	777
Toxicity	Low/None	None	None	Low/Med	None	Hazard	Low/None

Iodine is almost identical in mass to Xe, with a slightly larger electron-impact ionization cross section, and it is inexpensive. However, to its detriment, it is reactive with many substances.

Cesium is also almost identical in mass to Xe, but it has a much larger ionization cross section and a very low ionization potential. In fact, it can be contact ionized. However, it is toxic and very reactive. It was the earliest Hall thruster propellant,[5, 6] but by the mid 1960s, it was already being supplanted by the noble gases.[7]

Bismuth has a very large atomic mass and ionization cross section, and it stores at high density. Due to its large atomic mass and prospective efficiency, bismuth promises higher peak thrust-to-discharge power (T/P) than possible with xenon. It is also inexpensive and inert, and it has a relatively low melting point. Soviet era literature reports very high thruster efficiencies were achieved with bismuth.[8] In support of Project Prometheus, NASA funded Busek and a separate team including Stanford, JPL, TsNIIMASH, and Marshall Space Flight Center[9] to investigate bismuth thrusters. The Stanford/JPL team used a Russian thruster developed by TsNIIMASH, while Busek developed its own.[10] The Michigan Technical University is also studying Bi thrusters.[11]

The Achilles heel of bismuth is its low vapor pressure. To prevent condensation, wetted surfaces inside the thruster must be pre-heated and maintained at temperatures of 700 C or higher. The vapor is produced at even higher temperatures. This presents design challenges and potential reliability issues. The low vapor pressure is also a spacecraft interaction issue; significant amounts of bismuth may condense on some spacecraft surfaces. To address that issue, Busek commissioned The Aerospace Corporation to conduct a bismuth thruster spacecraft interactions study.[13] The conclusions were cautiously positive.

In the research described in this paper, Busek investigated magnesium and zinc. Vapor pressures for these elements, which are plotted in Figure 1, are much larger than the vapor pressure of bismuth. Consequently, magnesium and zinc thrusters should be much easier to design, test, and integrate with a spacecraft than bismuth thrusters. Moreover, these substances are atomically lighter than krypton, which means high I_{sp} may be achieved at relatively low voltages.

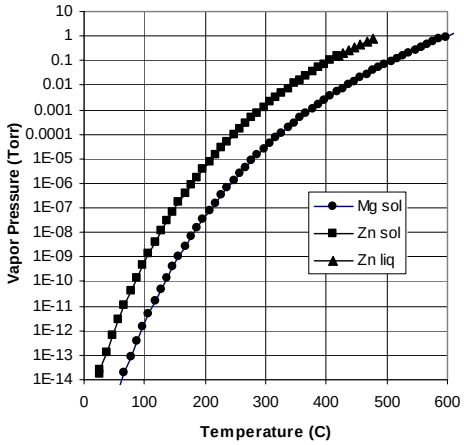

Figure 1. Vapor pressures of Mg and Zn.[12]

Magnesium is atomically the lightest of the substances in Table 1. It is only one fifth the mass of Xe. It also has a low first ionization energy and a very large ionization cross section. Mg Hall thrusters tested in the Soviet Union demonstrated efficiencies of ~50%.[2] The storage density is similar to that of Xe, but it can be stored as a solid and is relatively benign. Mg can also can be used to fuel a rocket, and it may be readily collected in-situ elsewhere in the solar system.

Zinc is the next lightest substances in Table 1. It is roughly half the mass of Xe, but it has a lower ionization energy and a comparable ionization cross section. The storage density is four times that of Xe, and it can also be stored as a solid. Like Mg and Bi, it is relatively benign. Busek first proposed Zn propellant to NASA in 2005.

C. Specific Impulse Predictions

According to the rocket equation, the change in velocity (ΔV_{sc}) that can be imparted to a space vehicle for a given fuel ratio ($\Delta m / m_o$) is proportional to I_{sp}. Table 2 is a low order estimate of the anode I_{sp} that may be achieved with various alternatives to Xe. This table assumes all the propellants are monatomic and that $I_{sp} \propto \sqrt{V_d / M}$, where M is the atomic mass. I_{sp} is scaled to 1800 s at 300 V, taken to be the baseline performance of a Xe thruster. At V_d=300 V, we predict I_{sp}~2600 s for Zn, and I_{sp}~4200 s for Mg. At V_d=250 V, we predict I_{sp}~2300 s for Zn, and I_{sp}~3800 s for Mg. At V_d=400 V, we predict I_{sp} ~ 3000 s for Zn, and I_{sp} ~ 4900 s for Mg.

Table 2. Scaled I_{sp} estimates for Xe, Zn, and Mg

		Predicted Isp (s) at Vd =		
Element	**A**	**250 V**	**300 V**	**400 V**
Xe	131	1643	1800	2078
Zn	65	2333	2555	2951
Mg	24	3839	4205	4856

D. Unique Characteristics of Magnesium

Magnesium has two additional characteristics which may be unique among electrostatic propellants.

First, magnesium can be used to fuel a chemical rocket. The predicted I_{sp} when Mg is combusted with CO_2 is 210-220 s.[14] The predicted I_{sp} when Mg is combusted with steam is 275-295 s.[15] This could enable a multi-mode propulsion system where non-toxic, storable propellants are used to generate both high Isp and high thrust.

Second, magnesium is found on the surface of Mars and the Moon in the form of MgO, from which Mg can be extracted in-situ using identified methods.[16] By mass, MgO is an estimated 8.5% of the Martian regolith[17] and 9.2% of the lunar regolith.[18] Oxidizers may also be collected in-situ on Mars and the Moon.

An Earth-Moon-Mars exploration architecture including in-situ resource utilization, Mg rockets, and Mg Hall thrusters may be in our future.

II. Experimental Procedure

We performed a series of targeted experiments to prove the feasibility of Mg and Zn Hall thrusters. These experiments leveraged existing hardware and facilities. One goal was to demonstrate and characterize a Mg or Zn discharge. This goal was achieved; both Zn and Mg were demonstrated. Another goal was to demonstrate a wire-based feed system that could be integrated with a light metal thruster in the future. This goal was also achieved.

A. Magnesium Demonstration

Busek's BHT-1500 xenon Hall thruster[19] served as the starting design point for all of Busek's metal propellant thrusters. Our Bi, Mg, and Zn thrusters all share the same basic magnetic circuit (with some minor differences) and mean channel diameter. The BHT-1500 is a single stage design suitable for high voltage plasma discharges up to 2-3 kW in power. The exit of the discharge channel is lined with boron nitride, while the upstream portion is metallic. Figure 2 shows the BHT-1500 equipped with a Busek hollow cathode.

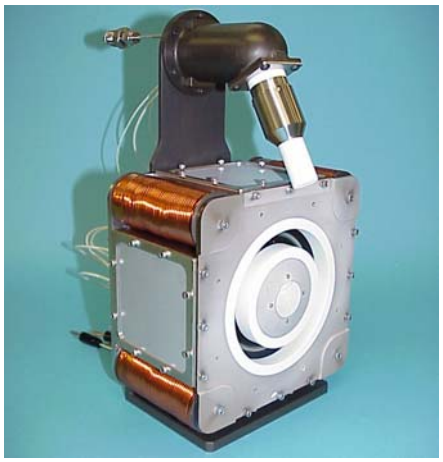

Figure 2. The BHT-1500 Hall thruster.

The magnesium demonstration concept is diagrammed conceptually in Figure 3. The magnetic circuit and anode were adapted from our vapor fed bismuth thruster. The system was designed to sublime the magnesium from a slug encapsulated upstream of the gas distributing anode. The feed rate is thus determined by the temperature of the slug. The system was designed such that heat could be added to the magnesium chamber through the use of a resistive element, enabling some control over the sublimation rate. Temperatures of the acceleration channel, anode, and evaporator tube were monitored with a series of electrically isolated thermocouples.

The system was placed on a thrust stand in front of a cooled beam dump in Busek's T8 facility, which provides approximately 180,000 l/s of xenon pumping speed. Figure 4 is an image of the Mg system viewed through the downstream end of the beam dump, which was capped by a glass sheet for the test. The thruster fires down the axis of the beam dump. The distance from the thruster exit plane to the entrance of the dump was approximately 6

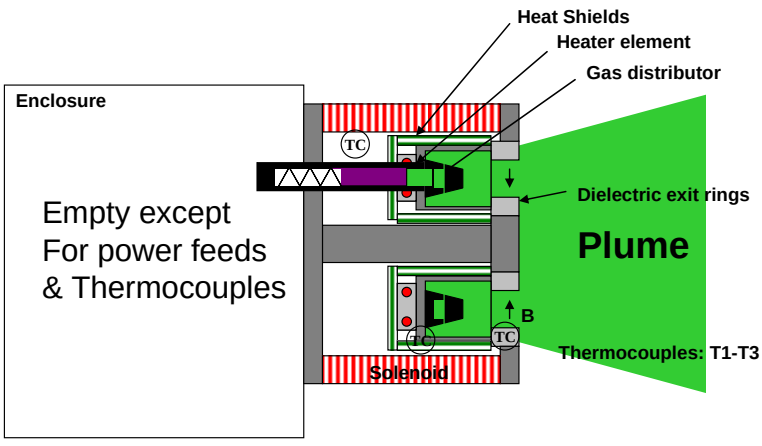

Figure 3. Magnesium demonstration system diagram.

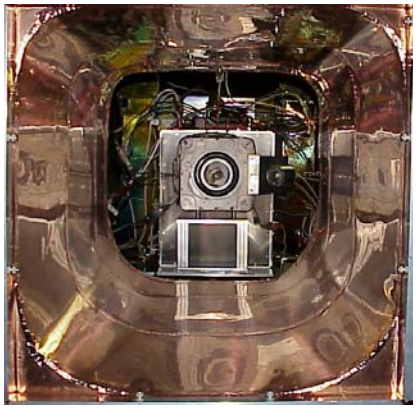

Figure 4. Magnesium demonstration system viewed through beam dump

inches. To neutralize the beam and provide electrons for the discharge, we used a Veeco hollow cathode flowing xenon. Mg/Zn cathodes are possible, but were beyond the scope of this demonstration.

To initiate the test, we pre-heated the vapor distributing anode to T > 600 C, which was required to prevent internal condensation. To achieve this temperature, we used both a resistive heater and a xenon discharge. The latter was turned off once magnesium vapor production became significant.

B. Zinc Demonstration

The zinc demonstration system, diagrammed in Figure 5, includes a complete propellant feed system. Vapor is produced at a separate, temperature controlled reservoir that is partially filled with condensed zinc. The reservoir and anode are connected by a heated line. Provided all downstream elements are hot enough to prevent condensation, the vapor feed rate to the anode is determined by the temperature at the reservoir.

It is important to note that Zn vapor could also be produced at an upstream reservoir on-orbit.

The zinc demonstration system was placed on a thrust stand and oriented in the same fashion as the Mg thruster. However, for this demonstration, the interior of the beam dump was fitted with a conical diffuser, and the back of the beam dump was opened behind this, allowing xenon from the cathode to more easily escape.

The thrust stand was calibrated prior to testing, and the results were linear and repeatable.

The Zn demonstration followed a different procedure than the Mg demonstration. We did not pre-heat the anode with Xe. Instead, we resistively warmed the propellant reservoir, flow line, and anode, started the cathode, and then turned on the Zn discharge. This procedure could be followed with Mg in the future.

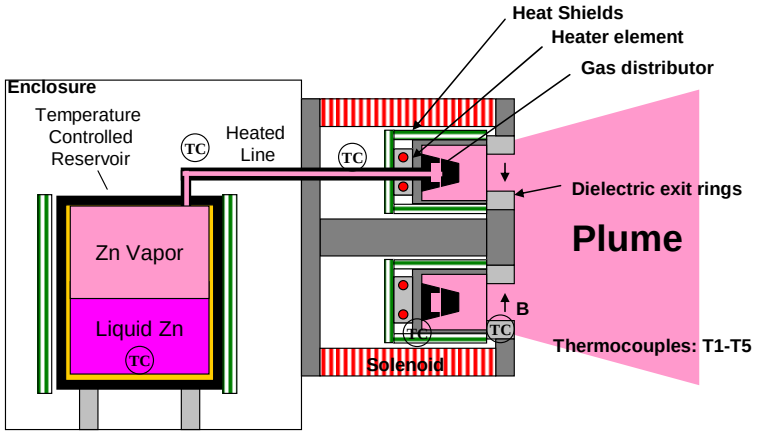

Figure 5. Zinc demonstration system

C. Wire Propellant Management System

Figure 6 shows the proof-of-concept wire propellant management system. A linear feed system meters the wire at a rate controlled by varying the voltage on a motor attached to a lead screw. The wire is fed into a 0.127" inner diameter cylindrical heater (on the left hand side of the picture) where it is vaporized. A gasket provides a seal between the wire and the upstream opening of the heater. The downstream "orifice" exhausts into a collection chamber. For Zn testing, the wire was wound on a spool. For the Mg test, the wire was actually a thin rod. Vaporization data were taken under vacuum.

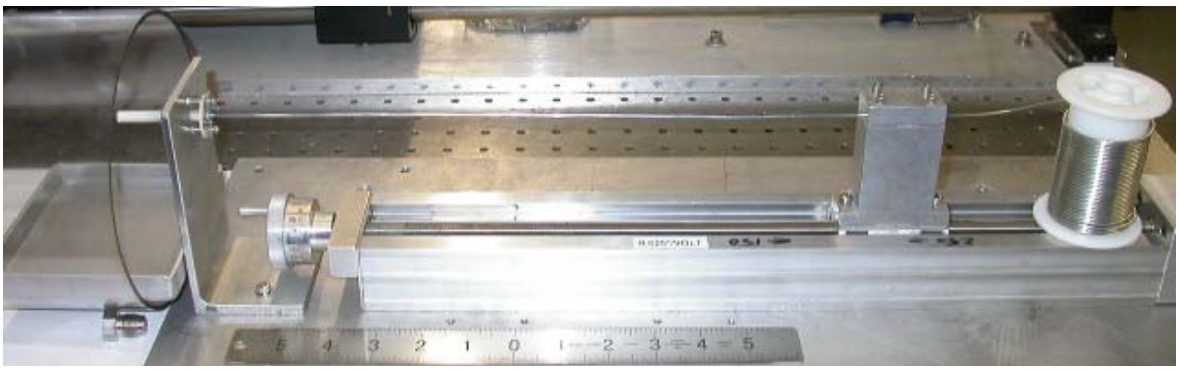

Figure 6. Proof-of-concept light metal wire propellant management system

Only a portion of the evaporator tube is actively heated, so a temperature gradient exists in the axial direction. Figure 7 is a temperature profile measured by a 1/6" diameter thermocouple translated along the axis. The thermocouple is not touching the walls. Position X=0 represents the downstream exit of the tube. The temperature is highest ¼" from the exit, which is the middle of the heated zone. In the entrance region, where the gasket is located, the temperature was T ≈ 300 C.

A thermocouple was placed on the outside of the tube so that we could monitor the gross temperature during testing. However, the position of this thermocouple was not fixed for all tests.

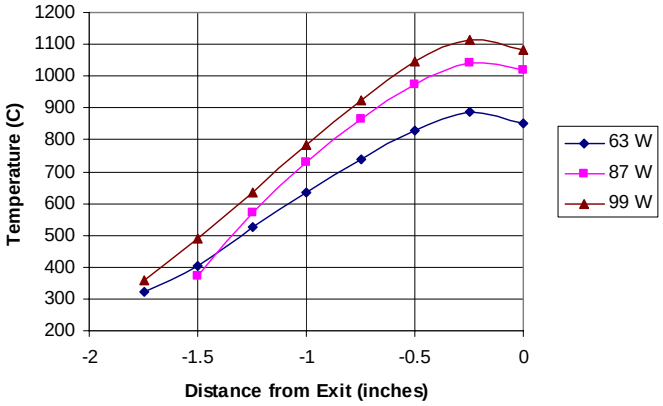

Figure 7. Temperature profile of evaporator tube.

III. Experimental Results

A. Magnesium Demonstration

Figure 8 shows the magnesium discharge. We have not yet produced a sharply defined jet. However, that may be a function of the operating conditions as well as the fact that the beam dump was capped.

Figure 10 shows the discharge current and inner magnet current during the initial portion of our first Mg discharge demonstration. For most of this period, the anode potential was 500 V. We believe the initial 1A discharge was fed by sublimation, which was the desired mode of operation. However, the current rose sharply at the same time the temperature near the Mg slug rose to 650 C, which is the melting point of Mg. The bottom of the anode filled with liquid magnesium, which then poured out into the discharge channel. The current through the inner magnet was varied in an attempt to control the current. However, the presence of liquid Mg in the discharge chamber made this task difficult.

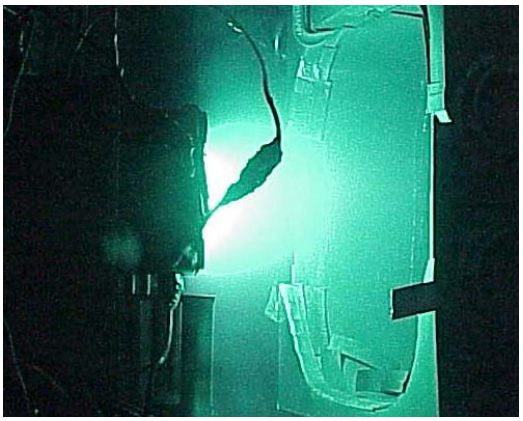

Figure 8. Magnesium HET plume.

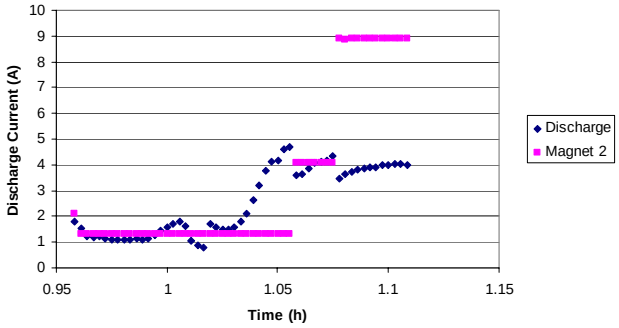

Figure 10. First magnesium demonstration.

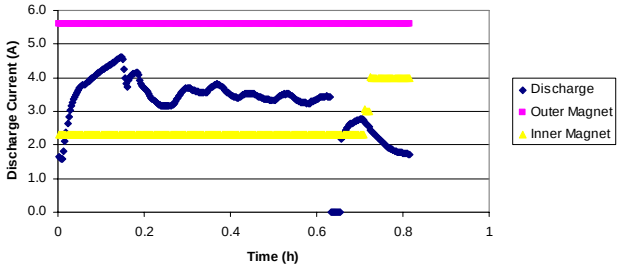

Figure 9. Second magnesium demonstration.

After the first demonstration, we disassembled the thruster and remove most of the solidified Mg. Unfortunately, some regions, such as the interior of the anode, were inaccessible. We then re-assembled the system without a slug in the vaporization chamber.

During the second test, the thruster was started as before. After turning the xenon off, the thruster exhibited the relatively steady conditions shown in Figure 9. After approximately half an hour of operating at a discharge current near 3.5 A and a discharge potential of 250 V, the current began to drop, indicating that the Mg was becoming exhausted.

At this point, we could have tested the Mg thruster

further. By simply orienting the thrust axis along with gravity (i.e. pointing the thruster upward) we could run this system without flowing liquid Mg into the anode. Alternately, through some simple design changes, we could either a) reduce the temperature at the slug, or b) restrain the Mg liquid, thus allowing thrust measurements. However, due to cost and time constraints, we moved on to Zn.

B. Zinc Demonstration

The critical difference between the Zn and Mg demonstrations was that the Zn reservoir was thermally isolated from the anode. Thus, the rate of vapor production was well controlled. The result was a very stable discharge allowing us to characterize the thruster.

We were able to start the Zn discharge on the first try without the use of a pre-heating xenon discharge. Figure 11 shows two views of the thruster firing into the beam dump. A beam jet is clearly visible. The color of the discharge is pink.

Figure 12 plots the discharge current (left) and discharge potential (right) during the course of the Zn discharge

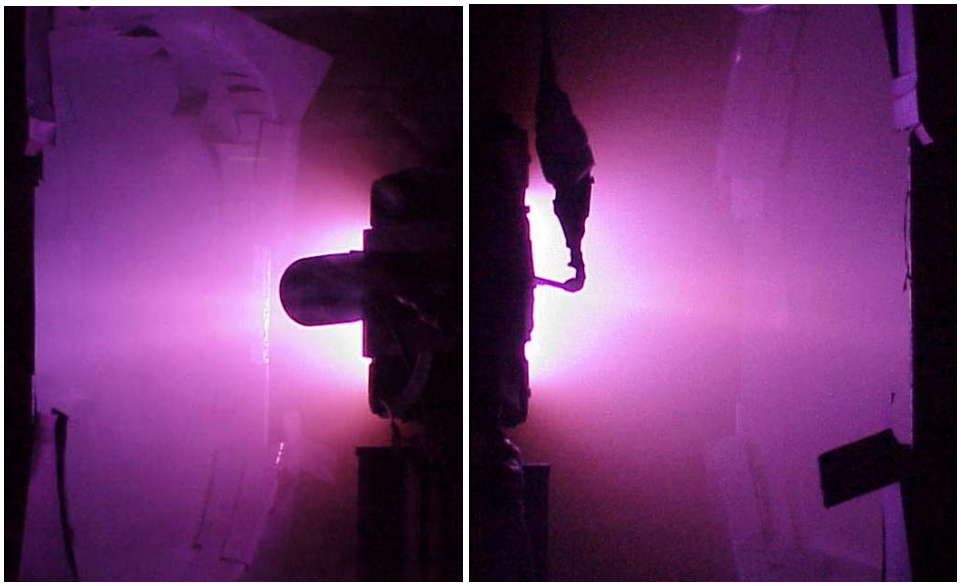

Figure 11. Zinc discharge demonstration.

demonstration test. Discharge current was supplied by a voltage regulated power supply. Most of the test was conducted at V_d=300 V. The discharge current, I_d, varied from 3.7 - 4.0 A for the majority of the test, indicating a nearly constant vapor feed rate. Thermocouple measurements indicate that the temperature of the Zn reservoir was nearly constant, though it was not regulated through an automated feedback control system.

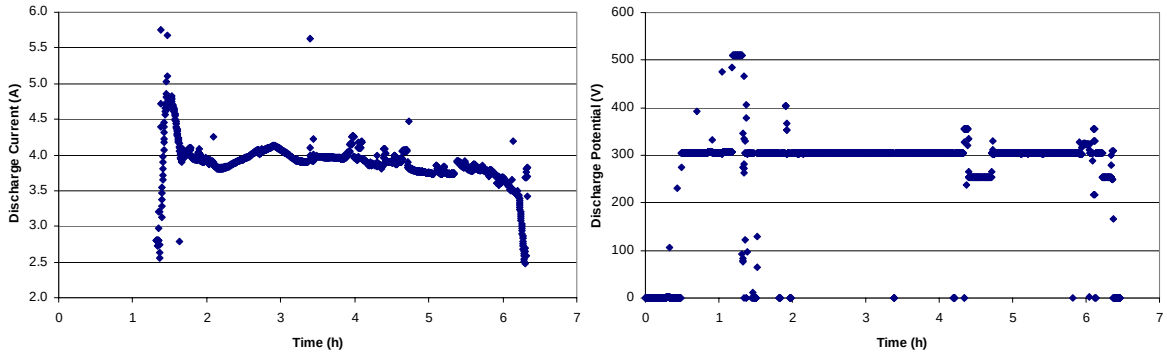

Figure 12. Discharge current (left) and discharge potential (right) during the Zn discharge demonstration.

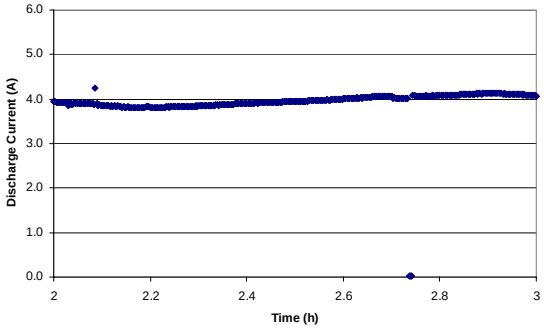

Figure 13. Duration test portion of the Zn demonstration

The Zn thruster as configured was more sensitive to magnet current than the BHT-1500 when it is operated on xenon. It was easy to extinguish the Zn discharge by adjusting the magnet current aggressively. However, it was also possible to run for long periods of time at steady conditions provided we did not make any large adjustments. Figure 13 shows a one hour period when we exercised restraint; the only outage occurred when we adjusted the magnet settings.

After establishing stability, we characterized the thruster. Figure 14 shows the discharge current at V_d=250 V and V_d=300 V as the current through the magnets, I_m, was varied. At 250 V, the discharge was very stable and a discharge current minimum was reached at $I_m \approx$ 3.8 A. At 300 V, the discharge had a tendency to go out when the discharge current reached its minimum. This occurred near I_m=3.6 A. At and above 350 V, the discharge was difficult to run for extended periods of time near the current minimum. Our experience with bismuth thrusters, which we are able to run steadily at higher voltages, tells us this was probably related to electrical arcing at resistive heater elements associated with the propellant reservoir, propellant line, or anode.

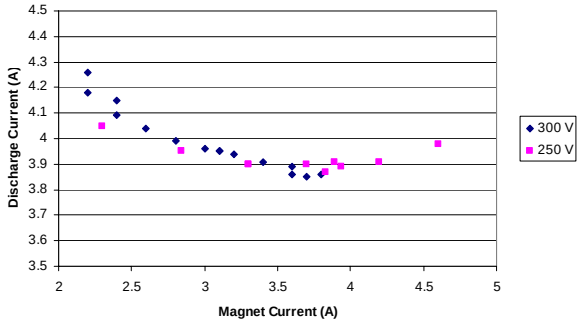

Figure 14. Zinc thruster discharge current variation with solenoid current.

A digital oscilloscope was used to measure discharge current oscillations. Measurements were taken at V_d=250, 300, and 350 V using a current monitor clamped onto the anode power lead near the power supply. At all voltages, the ionization ("breathing mode") oscillation was 21~23 kHz.

Table 3 contains performance data taken at V_d=250 V, where the discharge was most stable. Thrust, T, and discharge power, $P_d = I_d V_d$, were measured directly. The mass flow rate was estimated from the minimum discharge current using the following relation:

$$I_d \approx \frac{\dot{m} e Z}{M} \frac{\eta_u}{\eta_e}.$$

Here, η_u is the utilization efficiency, η_e is the electrical efficiency, and Z is the mean charge state of the ions. Based on BHT-1500 Xe thruster performance at Vd=250 and Vd=300 V, and assuming Z=1.1, we estimate that $0.9 < \eta_e / \eta_u < 1.0$. With $\eta_e / \eta_u = 0.95$ and Z=1.1, and assuming I_d=3.88 A, we estimate the flow rate is 2.26 mg/s +/- 0.1 mg/s. Given thrust, mass flow rate, and power, we can estimate specific impulse and anode efficiency:

$$I_{sp} = T / \dot{m} g_0;$$

Table 3. Measured and Estimated Performance of the Zinc Hall Thruster

Discharge Vd [V]	Discharge Id [A]	Magnets Im [A]	Measured Thrust [mN]	Discharge Power [W]	Discharge T/P [mN/kW]	Est. Anode Mass Flow [kg/s]	Est. Anode Isp [s]	Est. Anode Efficiency [%]	Thrust Error [%]	Isp Error [%]	Efficiency Error [%]
250	3.91	3.89	46.6	978	48	2.3E-06	2104	49	13	16	30
250	3.90	3.7	45.4	975	47	2.3E-06	2049	47	13	16	30
250	**3.89**	**3.94**	47.6	**973**	**49**	2.3E-06	**2148**	**52**	**13**	**16**	**30**
250	3.91	4.2	45.8	978	47	2.3E-06	2064	47	13	16	30
250	3.98	4.6	40.2	995	40	2.3E-06	1812	36	13	17	31
250	**3.87**	**3.83**	46.4	**968**	**48**	2.3E-06	**2091**	**49**	**13**	**16**	**30**
250	3.90	3.3	43.6	975	45	2.3E-06	1969	43	13	16	30
250	3.95	2.84	42.2	988	43	2.3E-06	1903	40	13	16	31
250	4.05	2.3	45.6	1013	45	2.3E-06	2056	45	13	16	30

$$\eta = T^2 / 2\dot{m}P_d .$$

With I_d minimized at V_d=250 V, the anode I_{sp} is about 2100 s and the anode efficiency is about 50%. The I_{sp} estimate is, within error bars, in agreement with the value in Table 2, which was 2300 s at V_d=250 V.

The three right hand columns in Table 3 show the normalized error associated with the thrust measurement and the I_{sp} and efficiency estimates. We assume the error in the mass flow rate estimate is +/- 10%. The error in the discharge power measurement is assumed to be 1%. The error in the thrust measurement is a combination of three different factors. The first is drift in the raw thrust stand voltage signal, which is minimized by periodically re-zeroing the thrust stand. The stand is equipped with an inclinometer, and we use its voltage signal to correct for small changed in inclination during the test. However, that correction is not perfect, so our second source of error is the uncertainty in the correction, which we assume may be off by 50%. This table also accounts for a third source of error – a bias voltage that appeared on the thrust stand signal when the discharge current oscillations were large. Only data points where the bias voltage is believed to be very small or nonexistent are included in Table 3. However, we include an additional 10% uncertainty factor on the thrust signal to be conservative. (Since these measurements were taken, the bias voltage error has been entirely eliminated.)

After taking into account all these error sources, the error bars become quite large. Therefore, further testing is required.

In this demonstration system, we require the anode heater to maintain temperatures high enough to avoid bismuth condensation. This parasitic heater power decreases the total efficiency of the system, which is not shown. However, through more careful thermal design, it should be possible to achieve desired anode temperatures using only the heat from the discharge.

An essential step sometime in the near future will be to establish the mass flow rate precisely. This could be achieved through the use of a wire based feed system.

C. Zinc Wire Vaporization

Table 4 summarizes the key Zn wire vaporization data. The feed rate was varied from $\dot{m}$ =1.0 to 4.0 mg/s, while the evaporator tube power was varied from 40 to 69 W. From Figure 7, the peak temperature in the tube in the latter case was about 900 C. The run time, Δt, was typically 40 minutes to an hour – long enough for a significant amount of wire to be processed. In all cases, a residue of zinc, M_r, was left in the tube after Δt, but the mass of wire that was vaporized was much greater than the mass of the residue. Taking the residue into account, we calculate a net vaporization rate, $\dot{m}_v = (\dot{m}\Delta t - M_r)/\Delta t$, which is included in the table. This calculation does not account for the time lag at startup between when the wire starts moving and when it reaches the vaporization zone, although this transient is less significant when the run time is longer.

The left side of Figure 15 shows the residue in the tube after Test 5, where the feed rate was $\dot{m}$ =2.0 mg/s and

Table 4. Experimental Zinc Evaporation Rates

FEED RATE [mg/s]	HEATER TEMP. [C]	POWER [w]	DURATION [min]	FEED MASS [g]	RESIDUE [g]	NET RATE [mg/s]	TEST number	TEST COMMENTS
1.0	515	43	70	4.2	1.18	0.7	7	no evidence of melt
1.0	525	40	30	1.8	1.84	0.0	8	reduced time,no melt
1.5	540	51	60	5.4	1.94	1.0	13	droplets found in vessel
2.0	520	42	48	5.76	1.84	1.4	5	melt droplet
2.0	580	44	45	5.4	1.74	1.4	9	melt drop at 540 C
3.0	600	58	29	5.22	1.39	2.2	10	vessel droplets
3.0	650	59	33	5.94	1.87	2.1	12	vessel droplets
4.0	635	69	24	5.76	1.47	3.0	11	vessel droplets

the heater input power was 42 W. The small diameter portion of the melt is where the Zn passed through the gasket. The large diameter portion represents the inner diameter of the evaporator tube. The melt terminates approximately

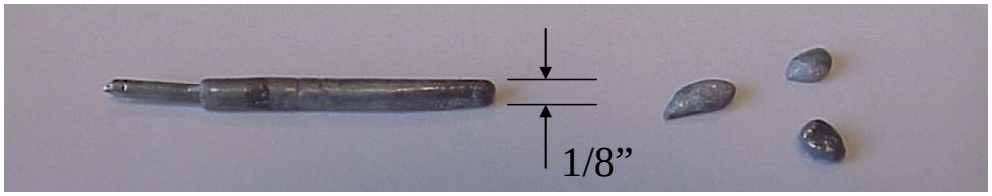

Figure 15. Zinc residue after vaporization test, including droplets found in vessel.

0.8" from the tube exit, near the onset of the high temperature region. It appears that the wire melted to fill the tube inner diameter, and vapor was created at the downstream surface.

Sometimes, at feed rates greater than 1.5 mg/s, droplets like those shown on the right side of Figure 15 were found inside the collection chamber after the test. Their time and place of origin is presently unclear. Although the tube exit seems the most probable source, the droplets were not located at or even near the exit of the tube. Furthermore, in most cases, no droplets were observed at the end of the evaporator tube during the test. However, the exit was not continuously observed.

In any case, it is very likely we reached a steady state where the feed rate is balanced by the vaporization rate at $\dot{m}$ =1.0 mg/s, where not droplets were found. At $\dot{m} \geq 1.5$ mg/s, the temperature may not have been high enough, as evidenced by the drops. We also note that there are large uncertainties in the $\dot{m}_v$ calculation at $\dot{m} \geq 1.5$ mg/s due to the drops (which were not included in the residue mass, M_r).

If the zinc wire feed system is integrated with a thruster, some provision should be made to guard against droplets breaking away from the meniscus and entering the anode. This could be as simple as a porous frit, as found in the SERT II Mercury ion engine.[20] Alternately, we may be able to design a Zn system that works entirely through sublimation. This certainly seems possible with Mg.

C. Magnesium Wire Vaporization

Table 5 summarizes the key Mg wire vaporization data. We saw no signs of melting and found no significant residue (other than the wire stub) inside the evaporator tube. After several lower temperature tests, we did find some small shreds of Mg in the downstream collection vessel. However, these were not present at higher temperatures. A small downstream screen would keep any such shreds from escaping through the anode of a thruster without being vaporized. To calculate a "net" vaporization rate, we weighed the Mg propellant rod before and after the test. The difference divided by the total test time, Δt , (including warm-up of the evaporator tube) was used to calculate a "net rate" of sublimation, which is included in Table 5. In all cases the net rate is slightly less than the feed rate, which we presently believe reflects time-lags in the system.

Figure 16 shows the end of the Mg rod as it appears after the end of a test. The Mg wire comes to a sharp point

Table 5. Experimental Magnesium Evaporation Rates

FEED RATE [mg/s]	HEATER TEMP. [C]	POWER [w]	DURATION [min]	FEED MASS [g]	NET RATE** [mg/s]	TEST number	TEST COMMENTS
0.42	600	56	28	0.71		1	no evidence of melt or vapor*
0.42	650/700	76	15	0.38		2	no vapor at 650, some shreding at 700
0.42	720	82	16	0.40		3	some shreads, vaporized 4" of rod
0.42	749	86	36	0.91	0.39	7	good test, reached limit of feed rod
0.65	800	110	12	0.47		4	vaporized 5" of rod*
0.65	850	97	24	0.94	0.60	6	good test, reached limit of feed rod
0.65	800	98	24	0.94	0.59	8	good test, some shreads, limit of feed rod
0.65	750	87	10	0.39		9	test ended, partially vaporized protruing rod
0.87	853	82	18	0.94	0.84	5	good test, reached limit of fed rod

** Calculated by weighing the Mg rod before and after the test and including total test-time including warm-up

inside the tube. This image also shows some small shreds found in the collection vessel. This particular sample was processed at a relatively low temperature.

From first principles, we were able to derive a set of equations that explains the "cone" shape of the Mg wire and

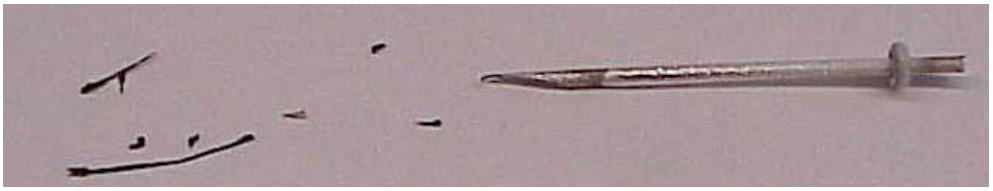

Figure 16. Mg wire after sublimation test, including shreds found in the vessel.

predicts with reasonable accuracy the required power levels and temperatures required to feed and sublime Mg wire at rate $\dot{m}$. These equations may be used to design in detail a wire-based feed system that avoids molten phases and feeds into an anode.

IV. Discussion

In the Phase I SBIR program reported here, Busek Co. Inc. demonstrated both zinc and magnesium Hall thruster discharges, as well as a wire-based feed system that could be integrated with the thrusters in Phase II.

We successfully demonstrated a Mg Hall thruster. Mg vapor was produced at a small reservoir attached to the anode. Our intention was to sublime the propellant, however, we exceeded the melting point of Mg. As a result, we only ran as intended for 4 to 5 minutes before liquid Mg appeared in the anode. In the future, we hope to fully characterize the thruster with propellant distributed entirely in the vapor phase.

We also successfully demonstrated a Zn thruster. Zn vapor was produced at a large, isolated reservoir and connected to the anode with an actively heated flow line. This architecture would be a viable option on the ground or in space for either Zn or Mg, though it would have to run at higher temperatures for the latter.

The Zn thruster started up easily and ran steadily for a long period of time, allowing us to characterize the system. Performance measurements and estimates indicate Zn thrusters are an efficient option for achieving high specific impulse at low discharge voltages. The measured thrust to power with a discharge potential of 250 V was ~49 mN/kW. The estimated specific impulse at 250 V, 1-kW was 2100 s +/- 340 s. The estimated anode efficiency peaks above 50%. A continuation of the test program is certainly warranted by these results.

A wire-based feed system was also successfully demonstrated at the proof-of-concept level. With Mg, we were able to sublime significant amounts of wire in a controlled fashion, reaching a steady-state where the feed rate was balanced by the evaporation rate. With Zn, the wire melted before it vaporized, but we still reached a steady-state at some flow conditions. We are looking forward to integrating the wire feed system with a thruster. It will provide us with exact knowledge of the mass flow rate to the thruster, enabling an accurate assessment of performance.

It is important to note that the power supplied to the evaporator tube in the wire feed system was much less than the overall discharge power enabled by the propellant flow rate. We created $\dot{m}$ =0.87 mg/s of Mg vapor using 82 W of power. We estimate that this flow rate is appropriate for a P_d~1800 W discharge at V_d~400 V. We also created $\dot{m}$ =3 mg/s of Zn vapor with 69 W of power (although there is some uncertainty associated with the vaporization rate). This is 20% higher than the estimated flow rate ($\dot{m}$ = 2.5 mg/s) for the Zn demonstration, which produced a P_d~1200 W discharge at V_d~300 V. The evaporator tube power represents a parasitic power loss, but it is small (on the order of 5% of the discharge power) and it is likely to get smaller. One of the chief power loss mechanisms is radiation, which would be greatly reduced if we added thermal shielding to the outside of the evaporator.

Further research is required to assess whether these systems can deliver high performance for extended periods of time and be successfully integrated with spacecraft.

V. Conclusion

Light metal Hall thrusters could provide both high I_{sp} and high efficiency at low voltage, enhancing or enabling many NASA missions.

These metals have favorable ionization properties, implying high efficiencies are possible. Because Zn and Mg are lightweight, high specific impulse is available at low voltage, enabling the use of existing power processors. Thus, these metals may reduce the mass and cost of interplanetary spacecraft. Zn and Mg thrusters may also be used for orbit raising, station-keeping, and repositioning. Life testing will be low cost because the vapors are self pumping; they condense on the vacuum chamber wall. Vapor pressure curves suggest minimal spacecraft interactions. Mg can also be combusted in a rocket, enabling a multi-mode propulsion system where the Hall thruster and rocket share propellant.

In the development program reported in this paper, we demonstrated Zn and Mg Hall thruster discharges and gathered a substantial body of experimental data including measurements of thrust and discharge current. The Mg thruster was not fully characterized, but Zn performance data are in-line with expectations. We also demonstrated a proof-of-concept wire-based propellant feed system and showed that it could efficiently meter useable amounts of Mg and Zn vapor. Taken together, our results prove the feasibility of using Zn and Mg as Hall thruster propellants.

Acknowledgments

The authors wish to acknowledge NASA for supporting the research.

Portions of the research described in this paper were carried out at the Jet Propulsion Laboratory, California Institute of Technology, under a contract with the National Aeronautics and Space Administration.

References

[1] D. Jacobson and D. Manzella, "50 kW Class Krypton Hall Thruster Performance," AIAA 2003-4550, 39th AIAA/ASME/SAE/ASEE Joint Propulsion Conference & Exhibit, June 20-23, 2003, Huntsville, Alabama.

[2] Tverdokhlebov, O. S. and Semenkin, A. V., "Iodine Propellant for Electric Propulsion – To Be Or Not To Be," AIAA 2001-3350, *37th Joint Propulsion Conference*, Salt Lake City, UT, July 2001.

[3]Gnedenko, V. G., Petrosov, V. A., Trofimov, A. V., "Prospects for Using Metals as Propellant in Stationary Plasma Engines of Hall-Type," IEPC-95-54, *24th International Electric Propulsion Conference*, Moscow, Russia, September 19-23, 1995.

[4]Kieckhafer, A. and King, L., "Energetics of Propellant Options for High-Power Hall Thrusters," AIAA 2005-4228, *41st AIAA Joint Propulsion Conference*, 10-13 July 2005, Tucson, Arizona.

[5]Seikel, G. R., and Reshotko, E., "Hall Current Ion Accelerator," *Bulletin of the American Physical Society*, Ser. II, Vol. 7, June 1962, p. 414.

[6]Seikel, G. R., "Generation of Thrust – Electromagnetic Thrusters," *Proceedings of the NASA-University Conference on the Science and Technology of Space Exploration*, Vol. 2, Nov. 1962, pp. 171-176.

[7]Janes, G. S., and Lowder, R. S., "Anomalous Electron Diffusion and Ion Acceleration in a Low-Density Plasma," *The Physics of Fluids*, 9, 6, June 1966.

[8]Grishin, S. D. and Leskov, L. V., *Electrical Rocket Engines of Space Vehicles*, Publishing House Mashinostroyeniye, Moscow, 1989.

[9] Sengupta, A. et al., "Summary of the VHITAL Thruster Technology Demonstration Program: A Two-Stage Bismuth-Fed VeryHigh Specific Impulse TAL", *30th International Electric Propulsion Conference ,Florence, Italy, September 17-20, 2007*

[10]Szabo, J., Gasdaska, C. Hruby, V, Robin, M. "Bismuth Hall Effect Thruster Development," *2005 JANNAF Propulsion Conference*, Monterey, CA, Dec 2005.

[11]D. Massey, L. King, J. Makela, "Development of a Direct Evaporation Bismuth Hall Thruster," AIAA-2008-4520, 44th AIAA/ASME/SAE/ASEE Joint Propulsion Conference & Exhibit, 21-23 July 2008, Hartford, CT.

[12] Alcock, C. B., "Vapor Pressure of the Metallic Elements," *CRC Handbook of Chemistry and Physics*, 83rd Edition, CRC Press, Boca Raton, 2002-2003, pp. 4-134 to 136.

[13]Crofton, M. and K. Diamant, K., "A Preliminary Study of Contamination Effects in a Bismuth Hal Thruster Environment," AIAA 2005-4231, *41st Joint Propulsion Conference*, 10-13 July 2005, Tucson, Arizona.

[14]Linnell, J. and Miller, T. "A Preliminary Design of a Magnesium Fueled Martian Ramjet Engine." AIAA-2002-3788, *38th Joint Propulsion Conference*, Indianapolis, IN, 2002

[15]Miller, T. F., and Herr, J. D. "Green rocket propulsion by reaction of Al and Mg powders and water." AIAA-2004-4037, *40th Joint Propulsion Conference*, West Palm Beach, FL, 2004.

[16]Sadoway, D. R. "New Opportunities for Metals Extraction and Waste Treatment by Electrochemical Processing in Molten Salts," *J. Mater. Res.*, 10 (3), 487-492 (1995).

[17]Carr, M. et al. "The Geology of the Terrestrial Planets." NASA SP-469 (1984): 57.

[18]Heiken, G. H., Vaniman, D. T. and French, B. M., *Lunar Sourcebook: A User's Guide to the Moon*. Cambridge University Press, 1991.

[19] Szabo, J and Azziz, J. Y. "Characterization of a High Specific Impulse Xenon Hall Effect Thruster," IEPC-05-324, *29th International Electric Propulsion Conference*, Princeton University, 31 Oct – 4 Nov 2005.

[20] Kerslake, W., "Design and Test of Porous-Tungsten Mercury Vaporizers," AIAA-72-484, *AIAA 9th Electric Propulsion Conference*, Bethesda, MD, April 17-19, 1972.